Assessing luminosity correlations via cluster analysis: evidence for dual tracks in the radio/X-ray domain of black hole X-ray binaries

Elena Gallo,[1]⋆ Brendan P. Miller[1] and Rob Fender[2]

[1]*Department of Astronomy, University of Michigan, 500 Church Street, Ann Arbor, MI 48109, USA*
[2]*School of Physics and Astronomy, University of Southampton, Highfield SO17 1BJ*

ABSTRACT

The radio/X-ray correlation for hard and quiescent state black hole X-ray binaries is critically investigated in this paper. New observations of known sources, along with newly discovered ones (since 2003), have resulted in an increasingly large number of outliers lying well outside the scatter about the quoted best-fitting relation. Most of these outliers tend to cluster below the best-fitting line, possibly indicative of two distinct tracks which might reflect different accretion regimes within the hard state. Here, we employ and compare state of the art data clustering techniques in order to identify and characterize different data groupings within the radio/X-ray luminosity plane for 18 hard and quiescent state black hole X-ray binaries with nearly simultaneous multiwavelength coverage. Linear regression is then carried out on the clustered data to infer the parameters of a relationship of the form $\ell_r = \alpha + \beta \ell_x$ through a Bayesian approach (where ℓ denotes logarithmic luminosities). We conclude that the two-cluster model, with independent linear fits, is a significant improvement over fitting all points as a single cluster. While the upper track slope (0.63 ± 0.03) is consistent, within the errors, with the fitted slope for the 2003 relation (0.7 ± 0.1), the lower track slope (0.98 ± 0.08) is not consistent with the upper track or with the widely adopted value of $\simeq 1.4$ for the neutron stars. The two luminosity tracks do not reflect systematic differences in black hole spins as estimated either from reflection- or continuum-fitting method. Additionally, there is evidence for at least two sources (H1743−322 and GRO J1655−500) jumping from the lower to the upper track as they fade towards quiescence, further indicating that black hole spin does not play any major role in defining the radio loudness of compact jets from hard black hole X-ray binaries. The results of the clustering and regression analysis are fairly insensitive to the selection of subsamples, accuracy in the distances and the treatment of upper limits. Besides introducing a further level of complexity in understanding the interplay between synchrotron and Comptonized emission from black hole X-ray binaries, the existence of two tracks in the radio/X-ray domain underscores that a high level of caution must be exercised when employing black hole luminosity–luminosity relations for the purpose of estimating a third parameter, such as distance or mass.

Key words: accretion, accretion discs – black hole physics – methods: statistical – ISM: jets and outflows – radio continuum: general – X-rays: binaries.

1 INTRODUCTION

The existence of a tight, non-linear correlation between the radio and X-ray flux of hard state black hole X-ray binaries (BHBs) over a wide dynamic range was first reported by Corbel et al. (2003) for GX339−4 (see also Hannikainen et al. 1998). Reanalysing a series of quasi-simultaneous observations for a sample of 10 hard

state black holes, collected over different epochs and with different instruments, Gallo, Fender & Pooley (2003, hereafter GFP03) concluded that the same relation, with a slope of 0.7 ± 0.1, (i) was a general property of hard state black holes; (ii) had similar normalizations for all sources, or in other words, it could be generalized for radio and X-ray *luminosities* all the way from quiescence up to a few per cent of the Eddington X-ray luminosity, above which a transition to the thermal dominant state (see e.g. McClintock & Remillard 2006, for a review of X-ray states) is typically observed, along with quenching of the core radio emission (Fender et al. 1999;

⋆E-mail: egallo@umich.edu

Russell et al. 2011; see Fender 2006, for a review of radio properties of X-ray binaries). With the inclusion of the nearby quiescent black hole binaries A0620−00 (the faintest radio/X-ray detection in the relation; Gallo et al. 2006) and V404 Cygni at its lowest luminosity level (Corbel, Körding & Kaaret 2008), the slope has been more recently revised to a somewhat shallower value (0.58 ± 0.16).

As radio and X-ray luminosities are thought to trace different emission processes – namely self-absorbed synchrotron from downstream in the jet versus inverse Compton/optically thin synchrotron from the compact corona/jet base, respectively – the slope of the correlation has been interpreted as evidence that a dominant fraction of the X-ray spectrum of hard state BHBs is due to optically thin synchrotron emission from the jet base (Markoff et al. 2003). Broad-band (radio-to-X-ray) spectral fitting provides independent evidence that this might be the case for a variety of weakly accreting black holes, both stellar and supermassive (Markoff, Falcke & Fender 2001; Malzac, Merloni & Fabian 2004; Markoff & Nowak 2004; Markoff, Nowak & Wilms 2005; Migliari et al. 2007; Markoff et al. 2008; Maitra et al. 2009, 2011; Russell et al. 2010 – see e.g. Corbel et al. 2004 for a counterexample, however), although other possible interpretations of the scaling relation remain open (e.g. Maccarone 2005). Regardless of its physical explanation, the non-linearity of such 'universal' scaling implies the existence of an accretion regime where most of the accretion power is released (likely in the form of mechanical power) within the jet, as opposed to being dissipated locally within the accretion-corona system (as discussed in GFP03, this is simply as a result of the empirical 0.7 slope combined with the theoretical prediction that the radio power and the total jet power correlate with a 1.4 power-law slope in partially self-absorbed jet models; cf. Blandford & Königl 1979).

Migliari & Fender (2006) subsequently reported on a similar investigation for the neutron star systems, showing that a steeper (albeit less tight) correlation exists between the radio and X-ray luminosity in neutron stars, too, of the form $L_r \propto L_x^{1.4}$. Incidentally, the difference in the inferred slopes for the black holes and the neutron stars nicely combine such that, unlike the black holes, neutron stars never enter the 'jet-dominated' regime. If so, that could be sufficient to account for the observed gap in luminosity between quiescent black holes and neutron stars, without requiring the presence/absence of a solid surface (Fender, Gallo & Jonker 2003; see also Körding, Fender & Migliari 2006a).

A qualitatively similar relation, with a slope of 0.6 ± 0.1, has been reported between the optical–infrared (IR) and the X-ray luminosity of both BHBs and low-mass neutron star X-ray binaries while in the hard state (Homan et al. 2005; Russell et al. 2006; Coriat et al. 2009), indicating a non-negligible contribution from the jet to the near-IR flux in these systems, although the relative contributions from jet versus reprocessed disc emission vary greatly between the two types of sources. Interestingly, there appears to be a hysteresis effect in the near-IR/X-ray correlation of hard state BHBs, namely, at a given X-ray luminosity, the near-IR emission appears to be weaker during the rise of an outburst than during the decline of an outburst (Russell et al. 2007).

Expanding on those works, two separate groups examined the possibility that similar scalings hold for supermassive black holes in active galactic nuclei (AGN) of the radio-weak variety, i.e. the AGN subclass whose properties most closely resemble those of hard state BHBs (e.g. Maccarone, Gallo & Fender 2003; Körding, Jester & Fender 2006b). Merloni, Heinz & di Matteo (2003) and Falcke, Körding & Markoff (2004) independently came to the same conclusion that weakly accreting black holes – from stellar mass scales to supermassive – preferentially lie on a plane in the three-

dimensional parameter space defined by their mass, nuclear X-ray luminosity and radio luminosity (see Körding, Falcke & Corbel 2006c; Merloni et al. 2006; Li, Wu & Wang 2008; Gültekin et al. 2009; Yuan, Yu & Ho 2009; Miller et al. 2010 for more recent studies). While the physical explanation for this finding is non-trivial (see e.g. Heinz 2004; Heinz & Merloni 2004; Plotkin et al. 2012), the best-fitting relation for this 'Fundamental Plane of black hole activity' may be employed for estimating or predicting one of the three observables (most notably mass) based on measurements of the remaining two (see e.g. Miller & Gültekin 2011; Reines et al. 2011 for two recent as well as remarkable examples).

Going back to the stellar mass black holes in X-ray binaries, measurements of radio and X-ray flux for newly discovered sources are similarly employed to estimate their most likely distance based on their location with respect to the best-fitting relation in the radio/X-ray domain (e.g. Cadolle Bel et al. 2007; Paizis et al. 2011; Rodriguez et al. 2011). Despite its fairly broad impact, though, the initial picture of a tight universal radio/X-ray luminosity relation has slowly drifted towards a more complex scenario. An increasing number of 'outliers' (Gallo 2007) have been reported, defined as falling well outside the scatter about the original GFP03 best-fitting relation (see the next section for references). Most of these points tend to be clustered *below* the best-fitting relation (i.e. at lower radio luminosities for a given X-ray luminosity), leading to the suggestion that there may be two separate tracks in the radio/X-ray luminosity plane of BHBs, each representing a different mode of accretion within the hard state (e.g. Coriat et al. 2011; see also Rushton et al. 2010, restricted to GRS 1915+105).

Motivated by Occam's razor, this paper sets out to give a statistically rigorous answer to the question whether, in the face of an increasing number of outliers and uncomfortably large scatter, it still makes sense to refer to a universal radio/X-ray correlation for hard state BHBs. The reader is referred to Xue & Cui (2007) for a different approach.

2 SAMPLE DESCRIPTION

We consider a sample comprised of multiple, *quasi-simultaneous* (i.e. within a day) radio and X-ray observations of 18 BHB systems while in the hard X-ray state, for a total of 166 data points (157 detections and nine upper limits in radio luminosity). In addition to the original sample of hard state BHBs discussed in GFP03 (nine sources excluding Cygnus X-1[1]), the following nine are included: XTE J1650−500 (data from Corbel et al. 2004), XTE J1908+094 (data from Jonker et al. 2004), A0620−00 (data from Gallo et al. 2006), XTE J1720−318 (data from Brocksopp et al. 2005, 2010), GRO J1655−40 (data from Migliari et al. 2007; Calvelo et al. 2010), IGR J17177−3656 (data from Paizis et al. 2011), Swift J1753.5−0127 (data from Cadolle Bel et al. 2007; Soleri et al. 2010), H1743−322 (data from McClintock et al. 2009; Jonker et al. 2010; Coriat et al. 2011) and IGR J17091−3624 (data from Rodriguez et al. 2011). In addition, new data points are included for 4U 1543−47 (data from Kalemci et al. 2005) and V404 Cygni (data from Corbel et al. 2008). A plot of radio luminosities (calculated by integrating up to the observed frequency and assuming a

---

[1] Data points relative to the high-mass BHB Cygnus X-1 are excluded from this analysis (as they were from GFP03) on the basis of its repeated 'failed' state transitions. See e.g. Rushton et al. (2012), discussing the peculiar radio behaviour of this source.
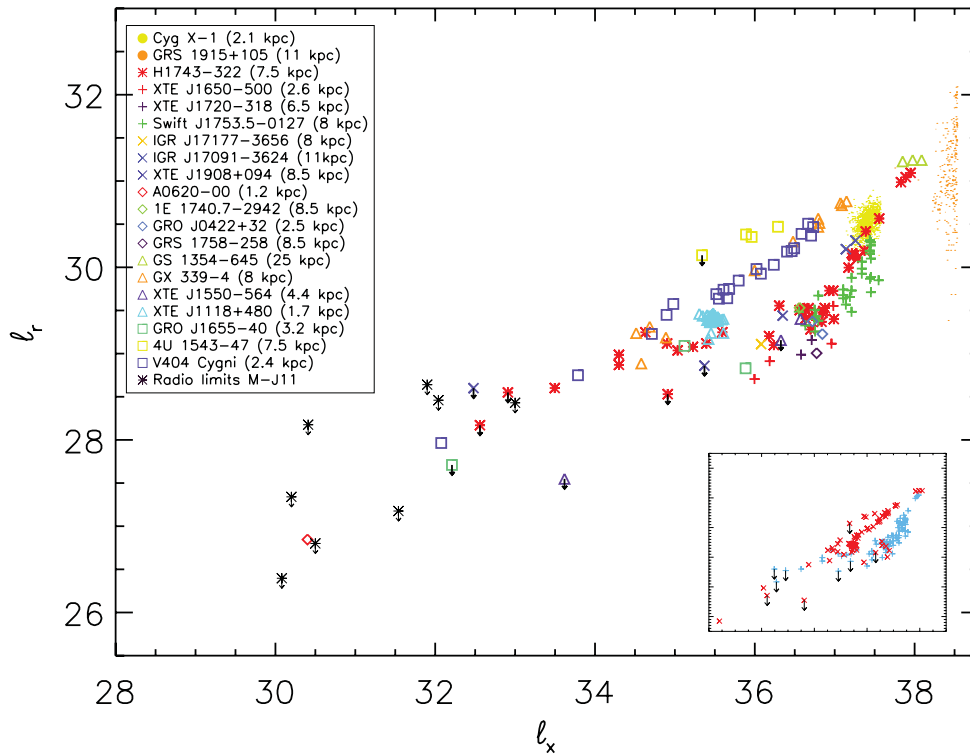
Figure 1. The full data set includes 165 hard state observations of 18 different X-ray binaries (XRBs), with radio and X-ray luminosities as indicated. Cygnus X-1, GRS 1915+105, along with the radio upper limits (combined with strictly non-simultaneous X-ray detections) by Miller-Jones et al. (2011) are plotted for illustrative purposes but are not included in our analysis (see the text). ℓ denotes log luminosities in units of erg s^{-1}. For the 18 sources under analysis, the inset illustrates luminosities for the sources with secure distance measurements, in red, versus uncertain distance measurements, in blue.

flat spectrum) versus 1–10 keV X-ray luminosities[2] for the 18 hard state BHBs under consideration is shown in Fig. 1, whose label also includes the adopted distances. Data points from Cygnus X-1 and GRS 1915+105 are also included for comparison, along with the radio upper limits from a recent deep survey of quiescent BHBs carried out by Miller-Jones et al. (2011, hereafter M-J11), but for which simultaneous X-ray counterparts are based on archival X-ray detections, often from observations that were taken several years prior to the radio survey.

Several authors (e.g. Jonker et al. 2010; Rushton et al. 2010; Coriat et al. 2011; Ratti et al., submitted) have suggested that there appears to be dual upper and lower luminosity tracks in this domain, particularly when compared against fig. 2 of GFP03, where a single correlation was identified. For descriptive purposes, the divide can be loosely set by the $\ell_{r} = \ell_{x} - 7$ line, where ℓ denotes log luminosities in units of erg s^{-1}. We investigate the effective validity of such a split classification in the following sections.

When available, luminosities have been updated based on recent and or more accurate distance measurements (based on the references in table 2 of Fender, Gallo & Russell 2010; Jonker & Nelemans 2004, except for the distance to XTE J1550−564 which has been recently revised to 4.4 kpc; cf. Orosz et al. 2011). Seven out of the 18 sources considered here (i.e. H1743−322, XTE J1650−500, XTE J1720−318, XTE J1908+094, Swift J1753.5−0127, IGR J17177−3656 and IGR J17091−3624) have less than reliable distance values, in that their distance determi-

tions are based on loose absorption arguments, or, in some instances, on their very location on the radio/X-ray luminosity plane investigated here. We refer to this subsample as 'uncertain distance' sample (versus 'secure distance sample'). The inset of Fig. 1 illustrates the locations of the two samples: note that culling objects with uncertain distance measurements removes the majority of the lower track data points (71 out of 77), although those six points that remain come from three distinct objects with secure distances (GRO 1655−40, XTE 1550−564 and GRS 1758−258).

3 CLUSTERING ANALYSIS

For the sample described above, we address three general questions: (i) whether there are necessarily two (or more) clusters populated within the $\ell_{r}-\ell_{x}$ plane; (ii) if so, what function optimally characterizes the clustering, and with which cluster is each individual observation most likely associated; (iii) given these groupings, is the single linear regression model derived from all observations consistent with the best-fitting lines within each cluster, and to what degree, if any, is the distinct-trends model statistically preferred. We wish to stress that the clustering analysis can only handle *detections*; we include the treatment of the upper limits in the linear regression analysis.

Potential clustering of observations within the radio/X-ray luminosity plane is investigated using standardized, *x*:*y* coordinates (as opposed to raw L_{r}:L_{x}). 'Standardization' is a way of scaling variables so that different variables, measured in different units and/or over different dynamic range, can be more easily compared. While both radio and X-ray luminosity for our sample are measured in erg s^{-1}, they are integrated over different energy ranges and likely

---

[2] For consistency with GFP03, unabsorbed luminosities quoted in different energy bands have been converted to 1–10 keV luminosities using WEBPIMMS and assuming a power-law spectrum with index $\Gamma = 2$.
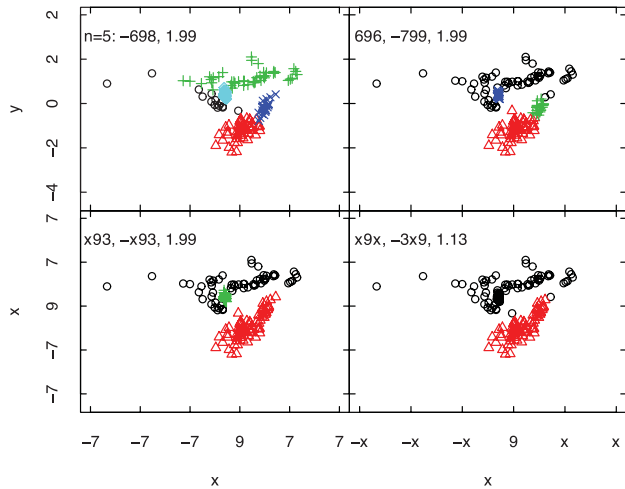
Figure 2. Model-based clustering results for $n = 2, 3, 4$ and 5 clusters (MCLUST code). Distributions are typically ellipsoidal, with varying enclosed area and orientations. Labels give the BIC and scaled-BIC values; models with the lowest (i.e. 1) scaled-BIC value are preferred.

account for different fractions of the bolometric luminosity emitted via their underlying emission process; in addition, the data set tends to stretch along the L_x-axis. The first transformation ($L_x \to x'$, $L_r \to y'$) includes taking the logarithm, subtracting the mean and dividing by the standard deviation, such that the resulting range of values for the primed coordinates is comparable along the x'- and y'-axes, while they both end up centred at $x' = y' = 0$. Principal component analysis (PCA; e.g. Jolliffe 2002) applied to x' and y' identifies the major component vector (essentially parallel to the upper track as defined above) to account for 87 per cent of the data variability. The data are rotated accordingly around their mean, such that they end up aligning with the principal component. The rotated variables are again scaled to unit variance, and clustering analysis is finally carried out on the resulting vectors, which we will refer to as x and y hereafter (see Fig. 2). This ensures comparable sensitivity (in terms of the ability to identify clusters) both along and across luminosity trends.

3.1 Model-based clustering

We first use MCLUST, a multivariate normal mixture modelling and model-based clustering code (Fraley & Raftery 2002, 2007), to evaluate the presence of n clusters, where n is allowed to vary from one to six. The considered models are spherical, diagonal or ellipsoidal distributions (permitted to vary in area, shape and orientation, where applicable), and models are ordered by likelihood as estimated using the Bayesian Information Criterion (BIC). BIC resolves the problem of 'overfitting' (increasing the likelihood of a model by adding parameters) by introducing a penalty term for the number of parameters in the model (it can be thought as an analogue to reduced χ^2 statistics in a clustering analysis framework). Given a series of models, the one with the higher BIC value is the one to be preferred (note that, by construction, BIC < 0).

Fig. 2 illustrates the results of this exercise by showing different clustering for $n = 2, 3, 4$ and 5 (bottom right, bottom left, top right and top left, respectively). At face value, three clusters, with ellipsoidal distributions, are preferred by the data (with a best-fitting BIC value of -695). For simplicity, the estimated BIC values can be scaled to the best-fitting BIC, such that a scaled-BIC value of unity corresponds to the best model. Fig. 3 illustrates the variation
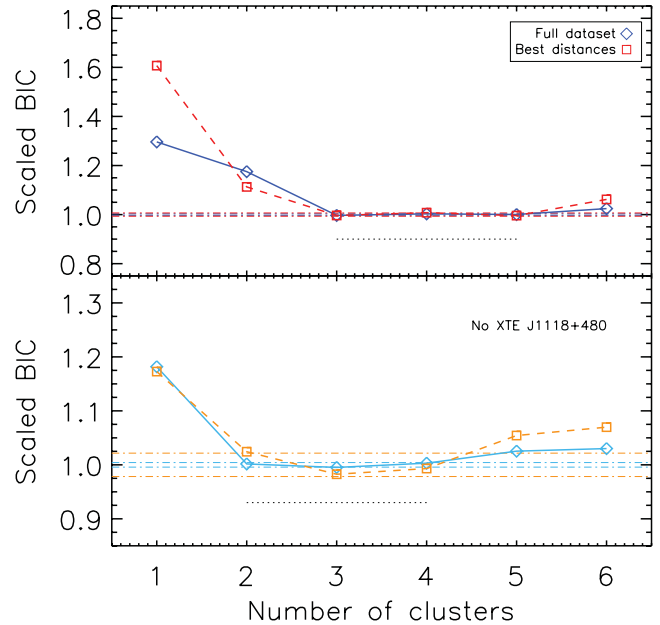
Figure 3. Scaled-BIC values (i.e. divided by the BIC value corresponding to the best-fitting cluster model) for $n = 1, 2, 3, \ldots, 6$ model-based clusters; dashed and dot–dashed lines are $1 \pm \sigma$ over the interval marked by the dotted segment. A measure of the preferred number of clusters is given by the leading edge of the plateau in scaled BIC. With (without) XTE J1118+480, three (two) clusters are preferred.

of such scaled-BIC value as a function of number of clusters for the full/secure distance samples. In this representation, a measure of the preferred number of clusters is given by the leading edge of the plateau in scaled BIC. While the two-cluster model (essentially identical to the upper and lower tracks as defined in Section 1) is associated with a slightly higher (1.18 versus 1) scaled-BIC value compared to the three clusters, it is clear that *two clusters provide a better description of the data set over a single-cluster model* (BIC value 1.18 versus 1.3, respectively). In addition, the three clusters consist of the upper and lower tracks as well as a separate grouping containing XTE J1118+480 points, which is likely distinguished by the particularly dense sampling over a very narrow dynamic range for this object, rather than any physical characteristics (for fitting purposes, the same XTE J1118+480 data points discussed here were actually averaged to a single data point in GFP03).

While four and five clusters (splitting the upper and then the lower track) do not provide an improvement over three, when restricting consideration to the subset of objects with secure distance measurements, the preferred three-cluster model again isolates most of the XTE J1118+480 points but now splits off the high-luminosity segment of the upper track while merging the low-luminosity segment of the upper track with the (here sparsely populated) lower track.

In summary, this method identifies three clusters – one corresponding entirely to the low dynamic range/high cadence XTE J1118+480 data – as preferred for the full data set and likewise for the subset of objects with secure distances, although in the latter case the groupings are not obviously related to the upper and lower tracks. When XTE J1118+480 is averaged to a single data point, two clusters (the upper and lower tracks) are preferred for the full data set, and perhaps also for the best distances subset (splitting off the high-luminosity segment of the upper track), although here three clusters (now separating out the lower track) do still have a slightly better BIC value.

An independent method of assessing clustering significance (also without the necessity of fixing a priori the clustering to be tested) is provided by the hierarchical Bayesian model implemented by Fuentes & Casella (2009; BAYESCLUST). BAYESCLUST allows to first test the null hypothesis (equivalent to just one cluster). It then proceeds to test the alternative hypothesis to be either two, three or four clusters at any one time. The assumed distribution for the observations is multivariate normal, and we use the default non-informative priors on σ (the variance) and μ (the mean for each cluster), with a minimum cluster size of 10 per cent of objects (i.e. 16 data points) enforced. BAYESCLUST adopts an importance sampling estimate for the Bayes factor by sampling from the partition distribution $g(\omega)$. The significance of clustering is then assessed through a frequentist approach, i.e. by simulating the distribution of the Bayes factors under the null hypothesis of a single cluster. The corresponding *p*-value, which gives a measure of the likelihood for one cluster, is 0.003, indicating again that two clusters are preferred over one. The suggested partitioning, however, is somewhat different from what is identified by MCLUST, in that a small fraction of the data points on the high-luminosity portion of the bottom track as identified by MCLUST are identified as members of the top track by BAYESCLUST.

3.2 Optimal clustering of observations

We further test and verify the model-based clustering presented above through applying three additional approaches: partitioning around medoids (Kaufman & Rousseeuw 1990; PAM), affinity propagation through iterative maximization of net similarity (Frey & Dueck 2007; implemented by Bodenhofer, Kothmeier & Hochreiter 2011, as APCLUSTER) and hybrid hierarchical clustering using mutual clusters (Chipman & Tibshirani 2006; HYBRIDHCLUST).

Both the *k*-means and *k*-medoids algorithms are partitional, i.e. break the data set into groups, and both minimize the distance between points labelled to be in a cluster and a point designated as the centre of that cluster, although partitioning around medoids is considered a more robust version of the standard *k*-means clustering algorithm in that it is more robust to noise and outliers. PAM is a classical partitioning technique that clusters the data set of *n* objects into *k* clusters, where *k* is a user-supplied parameter. When two clusters are requested, the code again separates out the upper and lower tracks.[3] As before, the most luminous points are included with the upper track, although they also appear potentially consistent with the lower track. When three clusters are requested, the upper track splits, but the high-luminosity end of the lower track also joins the high-luminosity segment of the upper track.

APCLUSTER (Frey & Dueck 2007) is a fairly new algorithm that takes as input measures of 'similarity' between pairs of data points and simultaneously considers all data points as potential cluster centres. In complex multidimensional problems, such as grouping images of faces, of genes identification, affinity propagation significantly outperforms even the best result of multiple *k*-means runs. Cluster centres are usually found by randomly choosing an initial subset of data points and then iteratively refining it, making the final result somewhat dependent on whether the initial choice is a fair representation of the whole data set. Instead, affinity propagation identifies exemplars (i.e. cluster centres) via 'message passing'

between points.[4] Messages are exchanged between data points until a high-quality set of exemplars and corresponding clusters emerge. Within the algorithm framework, adding a tiny amount of noise to the similarities to prevent degenerate situations (oscillations) corresponds to increasing the damping factor λ (allowed to vary between 0 and 1). High values of the preference *p* will cause affinity propagation to find many exemplars, while low values will lead to a small number of exemplars. Going back to our data set, low initial preference ($p = -100$) identifies again the upper and lower tracks; with higher preference ($p = -70$), the split occurs midway along and transverse to the upper track. Changing the damping factor from $\lambda = 0.9$ to 0.5 results in a slightly different membership for the three-cluster model.

Finally, we test a hybrid hierarchical clustering method that uses mutual clusters, where a mutual cluster is composed of points having a maximum relative distance less than the shortest distance to any point outside the group. HYBRIDHCLUST relies on the fact that bottom–up clustering cannot break a mutual cluster. That is, when agglomerating points, this method will never add points outside the mutual cluster before first joining all points inside the mutual cluster. The resultant top–down clusterings are then stitched together to form a single top–down clustering diagram, known as 'dendrogram', which allows to identify the number and composition of the clusters. The dendrogram for our data set is shown in Fig. 5, with insets illustrating the two and three cluster branches. The two primary clusters (splitting at a height of 300) are identified with the upper and lower tracks. The next two subclusters (splitting at a height of 140) dissociate the upper track into higher and lower luminosity portions.

Synthesizing the results from the previous two sections, *we conclude that two physically meaningful clusters are indeed significantly present in the radio/X-ray domain of hard state BHBs*, loosely corresponding to the upper and lower tracks as identified in Section 2, although the specific characteristics of the lower track in the full data set are influenced by objects with uncertain distances. It is worth noticing that the six most luminous points in the plot (corresponding to $\ell_r > 31$ and $\ell_x > 37$ in Fig. 1) are identified as members of the upper track by all clustering algorithms, whereas they could easily be classified as the upper luminosity end of the lower track in a more arbitrary 'by-eye' classification. In order to assess the robustness of our clustering analysis on measurement errors – which are not included in any of the routines discussed above – we verified that randomly scrambling the data points within a Gaussian of $\sigma = 0.15$ in ℓ_x and ℓ_r (i.e. a factor of 0.7–1.4 in flux, which may account for intrinsic source variability, lack of strict simultaneity, as well as measurement errors) still returns two clusters as the preferred model, and that the cluster membership is preserved.

We adopt the results described above to populate the cluster members for the linear regression analysis described in the following section. The two-cluster model – as identified by all methods except for BAYESCLUST – corresponds to the lower and upper tracks in e.g. the top inset of Fig. 5, while the three-cluster model typically subdivides the upper track, although it should be kept in mind

---

[3] Selecting from ℓ_x, ℓ_r rather than from *x*, *y* forms instead two groups split near $\ell_x = 36.3$.

[4] Two kinds of message are exchanged: (i) the 'responsibility' $r(i, k)$ (sent from data point *i* to candidate exemplar point *k*) reflects the accumulated evidence for how well-suited point *k* is to serve as the exemplar for point *i*, and (ii) the 'availability' $a(i, k)$ (sent from *k* to *i*), which reflects the evidence for how appropriate it would be for point *i* to choose point *k* as its exemplar, taking into account the support from other points that point *k* should be an exemplar (from Frey & Dueck 2007).
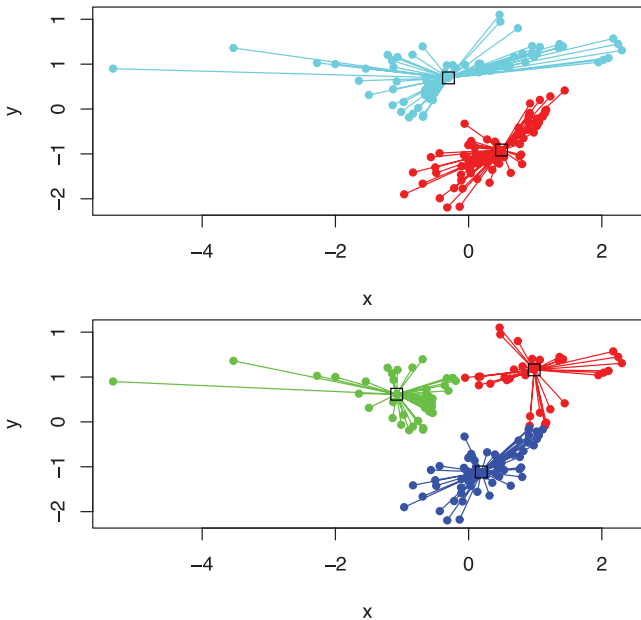
Figure 4. Clustering derived from affinity propagation (APCLUSTER) with initial preferences $p = -100$ and -70, respectively, for the top and bottom panels. The damping factor λ is set to 0.9 for both cases. The exemplars (i.e. cluster centres as identified by the code) are marked with squares.
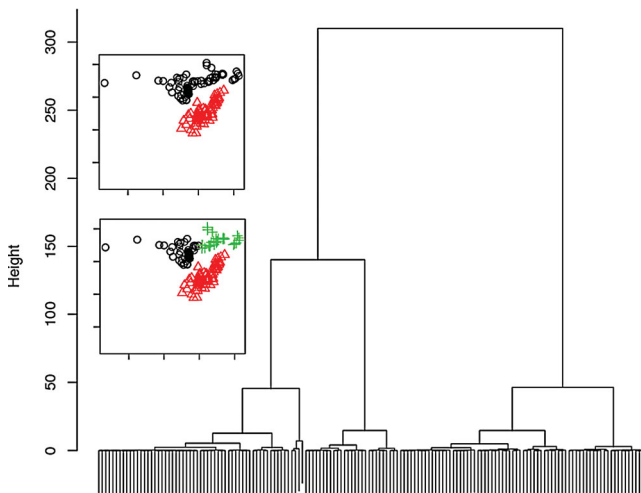
Figure 5. Dendrogram constructed through top–down hybrid hierarchical clustering, preserving mutual clusters (HYBRIDHCLUST). The inset shows the corresponding two and three cluster splits (which have been adopted for the linear regression analysis).

that various methods suggest somewhat different three-cluster splits (APCLUSTER and HYBRIDHCLUST return exactly the same groupings for the three-cluster model, as shown in the bottom panel of Fig. 4 and the bottom inset of Fig. 5, respectively). For the two-cluster model, the various algorithms (MCLUST, APCLUSTER, PAM and HYBRIDHCLUST) assign 86 and 71 data points to the upper and lower clusters, respectively. Restricting the selection to the secure distance subsamples returns 74 and six points.

4 LINEAR REGRESSION WITHIN CLUSTERS

We proceed to carry out linear regression on $(\ell_r - 29.5) = \alpha + \beta(\ell_x - 36.6)$, with intrinsic random scatter included. The centring

is based on the median luminosities in the full sample. Two Bayesian modelling packages are used to determine the parameters, the first from Kelly (2007; implemented in IDL as linmix_err.pro) and the second from Hall (2011; implemented in R as LaplacesDemon[5]), which serves for comparative purposes with analysis performed on the detections only.

The Kelly (2007) code permits input of measurement errors and optional dependent variable censoring. We assume uncertainties on both ℓ_x and ℓ_r of 0.15 dex. The radio upper limits are included in *all* fits, but fitting is also carried out using only the detected points for comparison and for χ^2 tests. Three Gaussians are used in the independent variable mixture modelling, and a minimum of 5000 iterations are performed with Gibbs sampling. The most likely parameter values are estimated as the *median* of 10 000 draws from the posterior distribution, with credible intervals corresponding to 1σ errors calculated as the 16th and 84th percentiles. The best-fitting models for each cluster are calculated separately.

The Hall (2011) code provides a framework for using adaptive Markov Chain Monte Carlo to optimize parameters for a user-specified model and priors. It constructs a linear model for which the prior probabilities of α and β within each considered cluster are taken to be Gaussian with mean zero. After each set of iterations, the program conducts self-diagnostics and if necessary suggests an additional run with modified sampling techniques to ensure convergence. The final runs consisted of 40 000–100 000 iterations, thinned to retain 1000 points. The most likely parameter values are again estimated as the medians. For the purpose of this work, the Hall code is employed in order to compare the results from the Kelly code with detections only (this is because the Hall code would require modifications in order to deal with upper limits and simultaneously evaluate the goodness of fit).

We consider three models: one cluster, two clusters or three clusters – the latter as identified by HYBRIDHCLUST and APCLUSTER. The various models are compared through both χ^2 versus degrees-of-freedom tests (implemented in IDL by Craig Markwardt as mpftest.pro), and through Laplace–Metropolis estimation of Bayes factors, for the Kelly and Hall codes, respectively. Both f-test (Kelly) and Bayes factor (Hall) calculations indicate that *the two-cluster model, with independent linear fits, is a significant improvement over fitting all points as a single cluster* (>99.9 per cent confidence). This is reflected in the highly reduced values of the intrinsic scatter, σ_0, which decreases from 0.40 for the one-cluster model to 0.22/0.11, respectively, for the higher and lower track fits for the two-cluster model. Results of the linear regression are shown in Figs 6 and 7. The slope of the linear fit to the upper track in the two-cluster model (from Kelly's code, including upper limits) is 0.63 ± 0.03, while the slope for the lower track is steeper, with 0.98 ± 0.08. The Hall code gives similar slopes, with 0.60 ± 0.04 and 0.88 ± 0.13, respectively, for the upper and lower tracks for *detected* points. The Kelly code returns consistent values with detections only: the fitted slopes are 0.61 ± 0.02 and 0.99 ± 0.08 (showing that the upper limits are almost completely uninformative for the lower track). This indicates that the few upper limits do not affect the results, providing support for the robustness of the clustering analysis from which they were necessarily excluded. However, we wish to stress that the uncertainties on the linear regression parameters are likely underestimated in that they are *conditional on the cluster identifications*.

---

[5] http://www.statisticat.com/laplacesdemon.html
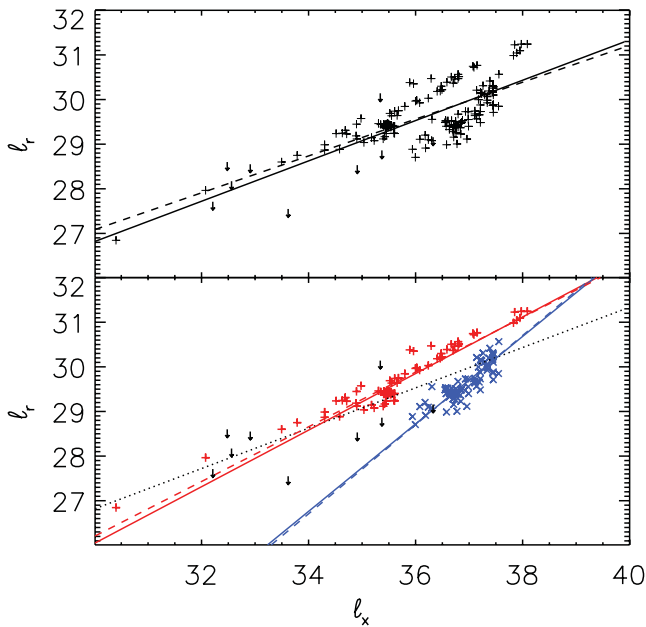
Figure 6. Results from the linear regression analysis, performed with the Bayesian modelling package of Kelly (2007). The solid (dashed) lines are computed for all data points (detections only). Top: full data set. Bottom: fit to two clusters. See Fig. 7 for details on the best-fitting parameters.

As an additional sanity check, we randomly selected two subsamples, with sizes corresponding to those of the two genuine clusters, and verified that in this case the dual line fit was properly rejected by both methods as a potential significantly improved model. The
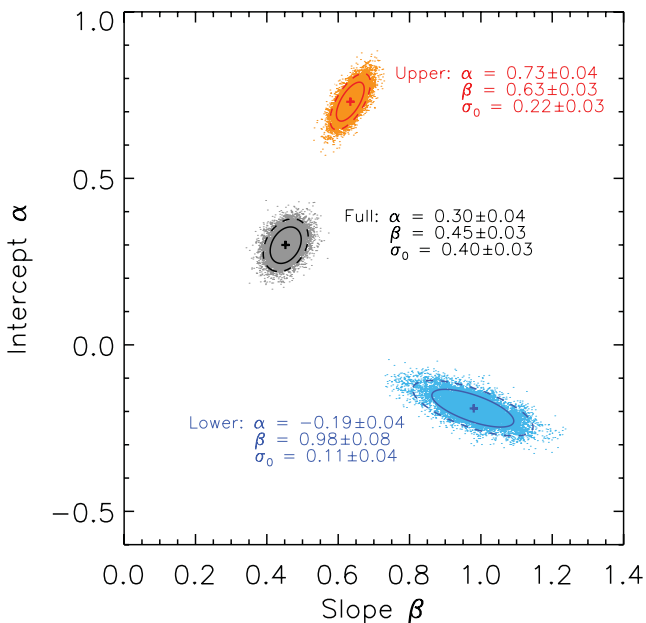
Figure 7. Results from the linear regression analysis conducted in Section 4 (using the code by Kelly 2007). The ellipses enclose 68 per cent (solid) and 90 per cent (dashed) joint confidence regions for the intercept (α) and the slope (β). The crosses are the best-fitting values. Quoted errors on the fitted intercept, slope and intrinsic scatter (σ_0) are at the 1σ level for one parameter of interest. Label colours correspond to the fitted models in Fig. 6, with black for the one-cluster model and red/blue for the upper/lower track in the two-cluster model. The intrinsic scatter is lower for the two-cluster model, with $\sigma_0 = 0.23/0.10$ versus $\sigma_0 = 0.40$ for the one-cluster model.

f-test calculations further suggest that the three-cluster model, with independent linear fits, is at most a marginal improvement ($p = 0.04$) over the two-cluster model and fits, although the Bayes factor suggests a more significant improvement. Regardless, the potential improvement for the three-cluster model is achieved through a flattening of the low-luminosity segment of the upper track, which may be influenced by the location of the many XTE J1118+480 points slightly below the upper track. Qualitatively similar results hold for the subset of objects with secure distance measurements, and in particular a separate line through the six lower track points provides a significant improvement to the overall fit.

5 SUMMARY AND DISCUSSION

Since the claim of a universal correlation between the radio and X-ray luminosity for hard state BHBs (GFP03), a more complex picture has emerged. With the addition of newly discovered sources, as well as new data from well-studied ones, the scatter about the 2003 best-fitting relation has been steadily increasing. In fact, the analysis presented here shows that, from a statistical point of view, *the existence of a single universal correlation between the radio and X-ray luminosity of hard and quiescent state BHBs is to be dismissed.* Our analysis, based on a number of clustering algorithms applied to nearly simultaneous radio/X-ray observations of 18 BHBs, shows that a two-cluster model, with independent linear fits, provides a better description of the data. The existence of two tracks does not depend on whether sources with highly uncertain distances are excluded from the analysis, although the actual functional form of the fits does, particularly for the lower track. The slope of the linear fit to the upper track (0.63 ± 0.03) is still consistent, within the errors, with the best-fitting slope (0.7 ± 0.1) given by GFP03 (later revised to a shallower $\simeq 0.6$ by Gallo et al. 2006 and Corbel et al. 2008), as well as with the fitted slope for the black hole Fundamental Plane (FP) relation (0.60 ± 0.11, although a small fraction of the BHB data considered here is generally included in the whole FP sample).The lower track slope (0.98 ± 0.08) is not consistent with the upper track or with the widely adopted value of 1.4 for the neutron stars (Migliari & Fender 2006).

These results are qualitatively insensitive to selecting subsamples, to the treatment of upper limits, and, we argue below, to accuracy in the source distances. Uncertain distances naturally tend to be equal to or larger than Galactic Centre distance, where absorption is more severe (this is true for six out of the seven sources in the uncertain distance sample, i.e. with the exception of XTE J1650−500[6]). Notwithstanding this effect, the lower track is very unlikely to be purely distance driven. If distances were systematically overestimated for the uncertain distance sample, this would make them even less luminous, effectively widening the divide with the upper track. On the other hand, as a result of the linearity in the lower track slope, inflating the uncertain distances of the lower track sample to yet larger values would shift the lower track towards higher luminosities *along* the $L_x \propto L_r$ line. The average distance of the uncertain distance sample would have to be increased to $\gtrsim 20$ kpc in order to have the lower track data points merge with the most luminous data points within the higher track, which seems unlikely, at least for *all* the lower track sources.

---

[6] The generally adopted distance of 2.6 kpc is simply based on the assumption that it reached a certain fraction of the Eddington luminosity during a soft-to-hard state transition (Maccarone 2003).

In our analysis, we purposely chose not to group data points belonging to the same source, such that the clustering analysis is somewhat blind to specific sources. An orthogonal approach is that followed by Soleri & Fender (2011), who, however, could not identify any obvious dependence of the BHB jet power (as traced by their radio luminosity) on the binary system parameters (i.e. orbital period, disc size, inclination) and/or outburst properties. Although Soleri & Fender are able to reproduce the large scatter observed in the radio/X-ray luminosity plane by inflating the jet bulk Lorentz factors to values larger than unity for X-ray luminosities above 10 per cent of the Eddington limit and assuming random inclinations, this scenario is admittedly contrived and even at odds with some of the measured inclination angles.

Rather than a single correlation with large scatter, the analysis presented here provides strong evidence for the existence of two tracks in the radio/X-ray luminosity plane. The actual cluster composition differs somewhat from that suggested by Coriat et al. (2011) based on visual inspection of the radio/X-ray luminosity plane for a subsample of BHBs plus the neutron stars, particularly when it comes to the top-right corner of the plane (specifically, Coriat et al. single out all of the H1743$-$322 high-luminosity points as belonging to their lower track – see fig. 5 in their paper; see also Kalemci et al. 2006; Jonker et al. 2010). Most importantly, the appealing suggestion that the lower track may be related to radiatively efficient accretion in the hard state strongly relies on a slope of $\sim$1.4 for the lower track,[7] which is not consistent with the value derived in this work based on a larger sample and more rigorous analysis.

Although there is no reason to believe that the two luminosity tracks may be a selection effect due to the lack of observational coverage in the gap, it should be noted that the lower track occupies a region of the parameter space at relatively high X-ray luminosities, a fact which led Coriat et al. (2011) to suggest that the two tracks may still collapse back to one at Eddington-scaled X-ray luminosities below $\sim$10$^{-3.5}$. While this seems to be the case based on the behaviour of H1743$-$322, which appears to have made a transition from the lower to the higher track as its X-ray luminosity decreased, there is a small but not negligible chance that the low X-ray luminosity, upper track data points for this source may actually correspond to unresolved optically thin radio ejections (see discussion in Jonker et al. 2010), rather than to partially self-absorbed core radio emission from a steady jet (if so, they ought to be discarded). Unfortunately, as discussed by M-J11, the current upper limits on the radio luminosities of most BHBs (see Fig. 1) make it impossible to establish whether the divide may also extend towards very low Eddington ratios, although the low upper limits on the radio luminosity of GRO J1655$-$40 and (particularly) XTE J1550$-$564 in quiescence reported by Calvelo et al. (2010) indicate that might be the case.

On the other hand, there are at least *two* sources that seem to be able to make transitions between the two tracks: beside H1743$-$322 (with the aforementioned caveats), GRO J1655$-$40, too, has two

simultaneous radio/X-ray detections each falling on either track (and so does the newly discovered XTE J1752$-$522; Ratti et al., submitted). While better sampling is clearly needed in order to make a stronger statement than based on a handful of data points, we conclude that there is *tentative evidence for sources being able to make transitions from the lower to the upper track as they fade towards quiescence*, although with no obvious parameter responsible for driving such a transition. While the option remains open that *some* of the lower track sources may actually be neutron stars, XTE J1550$-$564, XTE J1650$-$500 and GRO J1655$-$40 (only one out of two data points) all sit on the lower track, and all have confirmed black hole primaries (Greene, Baylin & Orosz 2001; Orosz et al. 2004, 2011), ruling out the possibility that *all* the sources on the lower track may be neutron stars. If confirmed, sources 'jumping' between the two tracks would further validate this statement.

We have no compelling explanation for this behaviour, not for the very existence of the two luminosity tracks. Hysteresis effects, of the same kind as reported for the near-IR–X-ray correlation by Russell et al. (2007), are not responsible for the observed pattern. As an example, GX339$-$4 is known to fall nicely on the upper track over repeated outburst cycles, both during the rise and the decline (e.g. Corbel et al. 2003). Casella & Pe'er (2009) ascribe the large scatter about the correlation to differences in the strength of the jet magnetic field from source to source. However, there is no straightforward explanation for a dual track behaviour in the context of this model (Pe'er & Casella 2009), nor for the jumping behaviour. Similarly, the existence of two tracks with different slopes is not expected within the jet-accretion models of Markoff et al. (2001, 2003) and/or Yuan & Cui (2005). The latter predicts that the slope of radio/X-ray correlation should become steeper ($\simeq$1.2), though at Eddington-scaled X-ray luminosities below $\lesssim$10^{-5} to 10^{-6}, while we observe dual tracks at Eddington-scaled X-ray luminosities above $\sim$10^{-4} (in this respect, deeper observations of quiescent BHBs are surely desirable in order to establish whether the lower track extends down to very low luminosities, as results by Calvelo et al. seem to indicate).

Finally, as also shown by Fender et al. (2010), the existence of two tracks within the radio/X-ray luminosity domain of BHBs cannot be possibly driven by two BHB subsamples with low and high spins. This conclusion remains valid even restricting the analysis to spin measurements from reflection-fitting methods alone (e.g. 4U 1543$-$47 is the most radio-loud source in our sample – in terms of radio to X-ray luminosity ratio – and has an inferred spin of 0.3 $\pm$ 0.1; the opposite is true for GRO J1655$-$40, on the lower track with an estimated spin value of 0.98 $\pm$ 0.01; Miller et al. 2009) or to thermal continuum fitting alone (e.g. A0620$-$00 lies on the low-luminosity end of the upper track, with a spin value of 0.12 $\pm$ 0.2 while GRO J1655$-$40 is on the lower track with a spin value between 0.65 and 0.75; Gou et al. 2010; Shafee et al. 2006, respectively). Furthermore, even in the absence of *any* spin measurement, sources jumping between tracks rule out the possibility that the black hole spin has a strong effect on the radio luminosity of the compact jet and hence on defining the two tracks, since the spin value of any given source cannot possibly vary on the typical time-scales of BHB outbursts [here we strictly refer to radio emission from the partially self-absorbed core radio jet observed in the hard state, a.k.a. compact jet – while it should be noted that a different conclusion has been drawn by Narayan & McClintock (2012), based on the luminosity peak of radio flares associated with hard-to-thermal state transitions].

Our results confirm and strengthen the conclusions of Soleri & Fender (2011) that the existence of two separate tracks in the radio/X-ray radio domain of BHBs does not reflect any obvious

---

[7] The suggestion that the lower track might be related to radiatively efficient accretion (Coriat et al. 2011) comes from the combination of (i) the theoretical scaling between the radio and the total jet power: $P_r \propto L_{jet}^{1.4}$ for partially self-absorbed jets (Blandford & König 1979; Falcke & Biermann 1996; Heinz & Sunyaev 2003); (ii) the empirical relation $L_r \propto L_x^{1.4}$. Under the assumption that the total jet power is directly proportional to the mass accretion rate, $\dot{m}$, the two scaling relations combine to give $L_x \propto \dot{m}$ for the lower track, characteristic of radiatively efficient accretion. Similarly, $L_r \propto L_x^{0.7}$ leads to $L_x \propto \dot{m}^2$ for the upper track, which would be indicative of radiatively inefficient accretion.

trend in any of the (known) physical parameters of the systems. The possibility remains open that the two tracks may reflect substantial differences in the actual average X-ray energy spectra. Pending availability of pointed X-ray observations with simultaneous radio coverage, a detailed X-ray spectral study could potentially highlight systematic differences between the two tracks, e.g. in terms of curvature in the hard X-ray spectrum and/or presence/absence of an optically thick disc (see Miller, Homan & Miniutti 2006; Cabanac et al. 2009; Tomsick et al. 2009; Dunn et al. 2011).

While a theoretical interpretation of this result is beyond the scope of this work, the existence of two tracks in the radio/X-ray luminosity domain of BHBs significantly hampers the predictive power of any X-ray binary radio/X-ray flux measurement for the purpose of mass and/or distance determination. Also, it should be kept in mind that these two tracks are not to be considered as analogues to the radio-quiet and radio-loud tracks (if any) for AGN: as demonstrated by Körding et al. (2006b) the entirety of the observations presented here – i.e. those of hard state BHBs – closely resemble AGN of the 'radio-quiet' variety, i.e. have moderate Eddington-scaled X-ray luminosities and fairly stable jets, with partially self-absorbed spectra reminiscent of compact extragalactic radio cores. By contrast, radio-loud AGN would be comparable to BHBs in the very high state, showing powerful and transient jet ejections with optically thin spectra, while black holes accreting between a few and 10 per cent of the Eddington X-ray luminosity are known to display a very different pattern radio/X-ray behaviour (e.g. Chatterjee et al. 2009; King et al. 2011 and references therein).

Further extrapolating these results to AGN and the FP of black hole activity, we argue that, while the measured scatter to the plane potentially allows for multiple tracks having comparable separations as the BHBs, dealing with a third parameter (and its large uncertainties) introduces a further level of complexity in the problem. Good prospects for breaking the mass degeneracy come from selecting a subsample of supermassive black holes with dynamically measured masses (Gültekin et al. 2009), since dramatically reducing the errors on the mass estimate results in a much tighter and better calibrated relation. An additional complication is introduced by the possibility that AGN obey the FP relation only in a time-averaged fashion (Miller et al. 2010), and that monitoring supermassive black holes on time-scales of months/years may introduce further deviations from the quoted best-fitting line, albeit not necessarily of the same nature as the dual tracks discussed in this work for BHBs.

REFERENCES

Blandford R. D., Königl A., 1979, ApJ, 232, 34
Bodenhofer U., Kothmeier A., Hochreiter S., 2011, Bioinformatics, 27, 2463
Brocksopp C., Corbel S., Fender R. P., Rupen M., Sault R., Tingay S. J., Hannikainen D., O' Brien K., 2005, MNRAS, 356, 125
Brocksopp C., Jonker P. G., Maitra D., Krimm H. A., Pooley G. G., Ramsay G., Zurita C., 2010, MNRAS, 404, 908
Cabanac C., Fender R. P., Dunn R. J. H., Körding E. G., 2009, MNRAS, 396, 1415
Cadolle Bel M. et al., 2007, ApJ, 659, 549
Calvelo D. et al., 2010, MNRAS, 409, 839

Casella P. G., Pe'er A., 2009, ApJ, 703, L63
Chatterjee R. et al., 2009, ApJ, 704, 1689
Chipman H., Tibshirani R., 2006, Biostatistics, 7, 268
Corbel S., Nowak M. A., Fender R. P., Tzioumis A. K., Markoff S., 2003, A&A, 400, 1007
Corbel S., Fender R. P., Tomsick J. A., Tzioumis A. K., Tingay S., 2004, ApJ, 617, 1272
Corbel S., Körding E., Kaaret P., 2008, MNRAS, 389, 1697
Coriat M., Corbel S., Buxton M., Bailyn C. D., Tomsick J. A., Körding E., Kalemci E., 2009, MNRAS, 400, 123
Coriat M. et al., 2011, MNRAS, 414, 677
Dunn R. J. H., Fender R., Körding E. G., Belloni T., Merloni A., 2011, MNRAS, 411, 337
Falcke H., Biermann P. L., 1996, A&A, 308, 321
Falcke H., Körding E., Markoff S., 2004, A&A, 414, 895
Fender R., 2006, Jets from X-ray Binaries. Cambridge Univ. Press, Cambridge, p. 381
Fender R. et al., 1999, ApJ, 519, L165
Fender R., Gallo E., Jonker P. G., 2003, MNRAS, 343, L99
Fender R. P., Gallo E., Russell D. M., 2010, MNRAS, 406, 1425
Fraley C., Raftery A. E., 2002, J. American Statistical Association, 97, 458
Fraley C., Raftery A. E., 2007, J. Classification, 24, 155
Frey B. J., Dueck D., 2007, Sci, 315, 972
Fuentes C., Casella G., 2009, Statistics Operations Res. Trans., 33, 115
Gallo E., 2007, in di Salvo T. et al., eds, AIP Conf. Ser. Vol. 924, The Multicolored Landscape of Compact Objects and Their Explosive Origins. Am. Inst. Phys., New York, p. 715
Gallo E., Fender R. P., Pooley G. G., 2003, MNRAS, 344, 60 (GFP03)
Gallo E., Fender R. P., Miller-Jones J. C. A., Merloni A., Jonker P. G., Heinz S., Maccarone T. J., van der Klis M., 2006, MNRAS, 370, 1351
Gou L. et al., 2010, ApJ, 718, L122
Greene J., Baylin C. D., Orosz J. A., 2001, ApJ, 554, 1290
Gültekin K., Cackett E. M., Miller J. M., Di Matteo T., Markoff S., Richstone D. O., 2009, ApJ, 706, 404
Hannikainen D. C., Hunstead R. W., Campbell-Wilson D., Sood R. K., 1998, A&A, 337, 460
Heinz S., 2004, MNRAS, 355, 844
Heinz S., Merloni A., 2004, MNRAS, 355, L1
Heinz S., Sunyaev R., 2003, MNRAS, 343, L59
Homan J., Buxton M., Markoff S., Bailyn C. D., Nespoli E., Belloni T., 2005, ApJ, 624, 295
Jolliffe I. T., 2002, Principal Component Analysis. Springer-Verlag, New York
Jonker P. G., Nelemans G., 2004, MNRAS, 354, 355
Jonker P. G., Gallo E., Dhawan V., Rupen M., Fender R., Dubus G., 2004, MNRAS, 351, 1359
Jonker P. G. et al., 2010, MNRAS, 401, 1255
Kalemci E., Tomsick J. A., Buxton M. M., Rothschild R. E., Pottschmidt K., Corbel S., Brocksopp C., Kaaret P., 2005, ApJ, 622, 508
Kalemci E. et al., 2006, ApJ, 639, 340
Kaufman L., Rousseeuw P., 1990, Finding Groups in Data: An Introduction to Cluster Analysis. Wiley, New York
Kelly B., 2007, ApJ, 665, 1489
King A. et al., 2011, ApJ, 729, 19
Körding E. G., Fender R. P., Migliari S., 2006a, MNRAS, 369, 1451
Körding E. G., Jester S., Fender R., 2006b, MNRAS, 372, 1366
Körding E., Falcke H., Corbel S., 2006c, A&A, 456, 439
Li Z.-Y., Wu X.-B., Wang R., 2008, ApJ, 688, 826
Maccarone T. J., 2003, A&A, 409, 697
Maccarone T. J., 2005, MNRAS, 360, L68
Maccarone T. J., Gallo E., Fender R. P., 2003, MNRAS, 345, L19
McClintock J. E., Remillard R. A., 2006, Black Hole Binaries. Cambridge Univ. Press, Cambridge
McClintock J. E., Remillard R. A., Rupen M. P., Torres M. A. P., Steeghs D., Levine A. M., Orosz J. A., 2009, ApJ, 698, 1398
Maitra D., Markoff S., Brocksopp C., Noble M., Nowak M., Wilms J., 2009, MNRAS, 398, 1638
Maitra D., Miller J. M., Markoff S., King A., 2011, ApJ, 735, 107

Malzac J., Merloni A., Fabian A. C., 2004, MNRAS, 351, 253

Markoff S., Nowak M. A., 2004, ApJ, 609, 972

Markoff S., Falcke H., Fender R., 2001, A&A, 372, L25

Markoff S., Nowak M., Corbel S., Fender R., Falcke H., 2003, A&A, 397, 645

Markoff S., Nowak M. A., Wilms J., 2005, ApJ, 635, 1203

Markoff S. et al., 2008, ApJ, 681, 905

Merloni A., Heinz S., di Matteo T., 2003, MNRAS, 345, 1057

Merloni A., Körding E., Heinz S., Markoff S., Di Matteo T., Falcke H., 2006, New Astron., 11, 567

Migliari S., Fender R. P., 2006, MNRAS, 366, 79

Migliari S. et al., 2007, ApJ, 670, 610

Miller J. M., Gültekin K., 2011, ApJ, 738, L13

Miller J. M., Homan J., Miniutti G., 2006, ApJ, 652, L113

Miller J. M., Reynolds C. S., Fabian A. C., Miniutti G., Gallo L. C., 2009, ApJ, 697, 900

Miller J. M., Nowak M., Markoff S., Rupen M. P., Maitra D., 2010, ApJ, 720, 1033

Miller-Jones J. C. A., Jonker P. G., Maccarone T. J., Nelemans G., Calvelo D. E., 2011, ApJ, 739, L18 (M-J11)

Narayan R., McClintock J. E., 2012, MNRAS, 419, L6

Orosz J. A., Steiner J. F., McClintock J. E., Remillard R. A., Corbel S., 2004, ApJ, 616, 376

Orosz J. A., Steiner J. F., McClintock J. E., Torres M. A. P., Remillard R. A., Bailyn C. D., Miller J. M., 2011, ApJ, 730, 75

Paizis A. et al., 2011, ApJ, 738, 183

Pe'er A., Casella P., 2009, ApJ, 699, 1919

Plotkin R. et al., 2012, MNRAS, 419, 267

Reines A., Sivakoff G. R., Johnson K. E., Brogan C. L., 2011, Nat, 7332, 66

Rodriguez J., Corbel S., Caballero I., Tomsick J. A., Tzioumis T., Paizis A., Cadolle Bel M., Kuulkers E., 2011, A&A, 533, L4

Rodriguez J. et al., 2008, ApJ, 675, 1436

Rushton A., Spencer R., Fender R., Pooley G., 2010, A&A, 524, 29

Rushton A. et al., 2012, MNRAS, 419, 3194

Russell D. M., Fender R. P., Hynes R. I., Brocksopp C., Homan J., Jonker P. G., Buxton M. M., 2006, MNRAS, 371, 1334

Russell D. M., Maccarone T. J., Körding E. G., Homan J., 2007, MNRAS, 379, 1401

Russell D. M., Maitra D., Dunn R. J. H., Markoff S., 2010, MNRAS, 405, 1759

Russell D. M., Miller-Jones J. C. A., Maccarone T. J., Yang Y. J., Fender R. P., Lewis F., 2011, ApJ, 739, L19

Shafee R. et al., 2006, ApJ, 636, L113

Soleri P., Fender R., 2011, MNRAS, 413, 2268

Soleri P. et al., 2010, MNRAS, 406, 1471

Tomsick J. A., Yamaoka K., Corbel S., Kaaret P., Kalemci E., Migliari S., 2009, ApJ, 707, L87

Xue Y. Q., Cui W., 2007, A&A, 466, 1053

Yuan F., Cui W., 2005, ApJ, 629, 408

Yuan F., Yu Z., Ho L., 2009, ApJ, 703, 1034

This paper has been typeset from a TeX/LaTeX file prepared by the author.